Journal of Zhejiang University-SCIENCE A (Applied Physics & Engineering)
ISSN 1673-565X (Print); ISSN 1862-1775 (Online)
www.jzus.zju.edu.cn; link.springer.com
E-mail: jzus_a@zju.edu.cn

Influences of fiber length and water film thickness on fresh properties of basalt fiber-reinforced mortar*

Leo Gu LI[1,2], Yi OUYANG[3], Pui-Lam NG[†‡2], Kai-long ZENG[4], Albert Kwok Hung KWAN[2]

[1]*Department of Civil Engineering, Guangdong University of Technology, Guangzhou 510006, China*

[2]*Department of Civil Engineering, The University of Hong Kong, Hong Kong 999077, China*

[3]*Mott MacDonald (Hong Kong) Ltd., Hong Kong 999077, China*

[4]*China Jinmao Holdings Group Ltd., Guangzhou 510030, China*

[†]E-mail: irdngpl@gmail.com

Received Sept. 7, 2020; Revision accepted Dec. 31, 2020; Crosschecked Apr. 7, 2021

Abstract: In plain mortar, the water film thickness (WFT) has been found to play a key role in the fresh properties. However, in fiber-reinforced mortar, the role of WFT has not been investigated yet. In this research, basalt fibers of different lengths were added to the mortar, and the dynamic and static flowability, cohesiveness, adhesiveness, and packing density were tested to study the effects of fiber length on the packing density and WFT, and the combined effects of fiber length and WFT on the fresh properties. The results showed that in fiber-reinforced mortar, the WFT also plays a key role, whereas the fiber length exerts its influences through the indirect effects on the packing density and WFT and the direct effect on fiber-mortar interaction. Basically, an increase in fiber length decreases the packing density and WFT, decreases the dynamic and static flowability needed for placing, increases the cohesiveness needed for avoiding segregation, and, quite unexpectedly, decreases the adhesiveness needed for rendering and spraying applications. Regression analysis yielded good correlation of the fresh properties to fiber length and WFT, and best-fit formulas for the mix design for basalt fiber-reinforced mortar were obtained.

Key words: Basalt fiber; Fiber-reinforced mortar; Fresh properties; Water film thickness (WFT)
https://doi.org/10.1631/jzus.A2000401 **CLC number:** TU528.58

1 Introduction

Utilization of different kinds of fibers to improve the mechanical performance and crack control capability of cementitious mortar/concrete has become a widely recognized technique (Gribniak et al., 2015; Chu et al., 2018; Li et al., 2019a). For fiber-reinforced mortar/concrete, there is no doubt that the fiber characteristics have great effects on the mechanical performance, and among the various characteristics, the fiber length appears to have the greatest effect. Ali et al. (2012) found that the strength of concrete with 5-mm long coconut fibers added was higher than those with either 2.5-mm or 7.5-mm long coconut fibers added. Abbass et al. (2018) observed that increasing the length of steel fibers would significantly improve the tensile and flexural strengths of the concrete. Eidan et al. (2019) revealed that the mechanical performance of concrete incorporating 12-mm long polypropylene fibers is generally better than that of the concrete incorporating 6-mm long polypropylene fibers.

‡ Corresponding author

* Project supported by the National Natural Science Foundation of China (Nos. 51608131 and 51808134), the European Regional Development Fund (No. 01.2.2-LMT-K-718-03-0010) under grant agreement with the Research Council of Lithuania (LMTLT), the Marie Skłodowska-Curie Actions of the European Commission (No. 751461), the Colleges Innovation Project of Guangdong Province (No. 2017KTSCX061), the Pearl River S&T Nova Program of Guangzhou City (No. 201906010064), and the Natural Science Foundation of Guangdong Province (No. 2021A1515011747), China

ORCID: Pui-Lam NG, https://orcid.org/0000-0003-0230-6874

In addition to influencing the mechanical performance, the fiber length also has salient effects on the fresh properties. Banfill et al. (2006) noted that decreasing the fiber length reduced the yield stress and plastic viscosity of carbon fiber-reinforced mortar. Poznyak et al. (2014) reported that increasing the fiber length increased the viscosity of basalt fiber-reinforced cementitious paste. Ghernouti et al. (2015) demonstrated that, when using plastic bag waste fibers in self-compacting concrete, increasing the fiber length adversely affected the passing ability. Islam and Ahmed (2018) revealed that, for a given fiber content, decreasing the length of jute fibers from 20 mm to 10 mm slightly decreased the slump. Overall, although it is well known that the presence of fibers affects the rheological behavior of mortar mixes, there has been little systematic research on the effects of fiber characteristics especially the fiber length on the fresh properties, as well as on the development of rheological models for fiber-reinforced mortar/concrete.

On the other hand, studies have been conducted to explore the key factors determining the fresh properties of cementitious mixtures (Banfill, 1994; Felekoğlu et al., 2007; de Schutter et al., 2008). Among the various factors, the water content is obviously the major one. The reason is that water plays a crucial role in lubricating the solid particles and imparting flowability to the water-solid mixture. Besides, both the particle packing (Powers, 1968; Yu et al., 1997; Kwan et al., 2012; Li and Kwan, 2014; Li et al., 2017a, 2021c) and the surface area of the solid ingredients (Claisse et al., 2001; Hunger and Brouwers, 2009; Cordeiro et al., 2011; Mehdipour and Khayat, 2017) have been proven to have major effects. This is because, for a given amount of water, a denser packing leads to more excess water being available to form water films on the solid particles whereas a larger surface area reduces the thickness of the water films and thus reduces the lubricating effect (Wong and Kwan, 2008; Kwan and Li, 2012, 2014; Ng et al., 2016).

From the above review, it is apparent that the influences of water content, packing density, and solid surface area are inter-related. Notwithstanding this, the amalgamated effects of these factors have been integrated into the water film thickness (WFT) parameter. Many researchers have found that the WFT is the principal parameter that governs the fresh properties of cementitious materials, including paste (Midorikawa et al., 2009; Wu et al., 2014; Li and Kwan, 2017; Chen et al. 2020), mortar (Kismi et al., 2012; Zhang and Panesar, 2017; Chen et al., 2019), and concrete (Li and Kwan, 2013; Ahari, 2018; Shi et al., 2018; Sun et al., 2018). Nevertheless, whether the concept of WFT is also applicable to fiber-reinforced paste/mortar/concrete requires further investigation. In particular, apart from the WFT, the role of the fiber length in the fresh properties also needs to be studied because the fibers, if relatively long, could affect the packing density and rheology of the cementitious material mixture (Li et al., 2017b, 2018a, 2018b).

This paper reports a comprehensive testing program on the roles of fiber length and WFT in the fresh properties of basalt fiber-reinforced mortar. The fresh properties tested included the dynamic and static flowability, cohesiveness, and adhesiveness of basalt fiber-reinforced mortar mixes with varying fiber lengths and water/cement ratios. Moreover, the packing density of each mortar mix was measured, and the WFT was calculated from the packing density and solid surface area of the mortar mix. From the test results, the effects of the fiber length on the packing density and WFT were studied, and the influences of the fiber length and WFT on the fresh properties were investigated by correlating the various fresh properties to both the fiber length and WFT.

2 Research details

2.1 Raw materials

Fine aggregate, cement, basalt fibers, and superplasticizer (SP) were employed as the raw materials. For the fine aggregate, river sand of 1.18-mm maximum grain size was used. For the cement, with a strength class of 42.5 MPa, ordinary Portland cement supplied by a cement production plant in Guangzhou and conforming to the prevailing Chinese standard GB 175–2007 (AQSIQ, 2007) was used. For the basalt fibers, they were imported from Ukraine and were made from molten basalt rock by a spinning process (Li et al., 2021b). The basalt fibers have a diameter of 16 μm and different lengths of 5, 10, 15, 20, and 25 mm. Basalt fibers with such diameter and lengths were standard products readily available from

the producer. Fig. 1 shows the basalt fibers used. Detailed information about the basalt fibers is presented in Table 1. It is clear that the fibers have desirable mechanical properties as well as good thermal and chemical stabilities. For the SP, an aqueous polycarboxylate-based formulation with a solid mass content of 20% was applied.

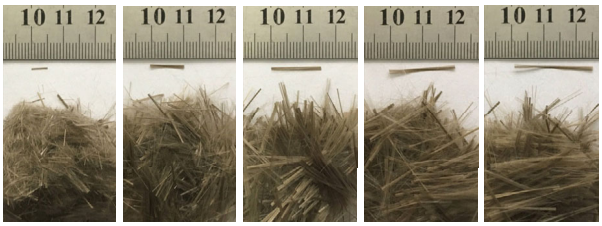

Fig. 1 Photographs of basalt fibers with different lengths

Table 1 Properties of basalt fibers

Property	Value
Elastic modulus (GPa)	84
Tensile strength (MPa)	1450
Elongation at break (%)	2.8
Fire blocking temperature (°C)	1200
Melting point (°C)	1350–1450

The specific gravity of each raw material is listed in Table 2. In the same table, the measured moisture content and water absorption of the river sand are also given. The particle size distributions (PSDs) of the river sand and cement are graphically presented in Fig. 2. From the respective PSDs of the river sand and cement, as well as the geometrical features of the basalt fibers, the specific surface areas (SSAs) of these materials are computed and presented in the last column of Table 2.

Table 2 Properties of raw materials

Material	Specific gravity	Moisture content (%)	Water absorption (%)	SSA (m^2/m^3)
River sand	2.58	0.04	1.10	$3.16\times10^{4*}$
Cement	3.12	–	–	$1.95\times10^{6*}$
Basalt fiber	2.53	–	–	2.50×10^{5}
SP	1.03	–		–

* It was assumed that the aggregate and cement particles are angular in shape like dodecahedrons having an SSA equal to 1.26 times that of spheres of the same size

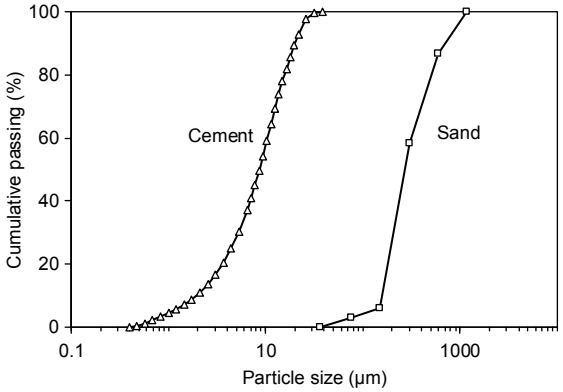

Fig. 2 Particle size distributions of cement and sand

2.2 Mix design

In total, 20 mortar mixes with different fiber lengths and various water/cement ratios were prepared for testing. The fiber lengths were 5, 10, 15, 20, and 25 mm, whereas the water/cement ratios were 0.25, 0.30, 0.35, and 0.40 by mass. In addition, the fiber content, expressed as a percentage ratio of basalt fibers to cement by mass, was set constant at 0.3% (equivalent to fiber content of 0.11% to 0.12% by volume of mortar). Based on preliminary trials, the aggregate/cement ratio was set at 1.0 by mass, and the SP dosage was fixed at 0.8% by mass of the cement content. Table 3 summarizes the mortar mix proportions. In this study, each mortar mix was labelled by a mix number in the form of *L*-*R*, in which *L* represents the fiber length (mm) and *R* represents the water/cement ratio, as listed in the first column of Table 3.

2.3 Testing methodology

A mini V-funnel test (Kwan et al., 2010) was used to assess the dynamic flowability in terms of the measured flow rate (in unit of mL/s calculated as the volume of mortar sample in the V-funnel divided by the flow time). Besides, a mini conical slump flow test (Okamura and Ouchi, 2003; Li et al., 2021a, 2021d) was applied to assess the static flowability in terms of the measured spread (the average diameter of the mortar after lifting the slump cone minus the base diameter of the slump cone) and the measured slump (the drop in height of the mortar after lifting the slump cone). Furthermore, a sieve segregation test using a 1.18-mm aperture sieve was carried out (Li and Kwan, 2011) to determine the cohesiveness. From the test,

the sieve segregation index (SSI) was obtained as the ratio of the mass of mortar dripped through the sieve and collected by the base receiver to the mass of mortar sample placed onto the sieve. The higher is the SSI value, the lower is the cohesiveness, and vice versa. It is noteworthy that the above mini conical slump flow test, mini V-funnel test, and sieve segregation test are actually reduced scale versions of the respective tests for fresh concrete mixes stipulated in the European standard EN 12350: Part 8 (CEN, 2019), Part 9 (CEN, 2010a), and Part 11 (CEN, 2010b).

Table 3 Mortar mix proportions

Mix number	Proportion (kg/m^3)				
	River sand	Cement	Basalt fiber	Water	SP dosage
5-0.25	1042	1042	3.12	260	8.33
5-0.30	990	990	2.97	297	7.92
5-0.35	943	943	2.83	330	7.55
5-0.40	901	901	2.70	360	7.21
10-0.25	1042	1042	3.12	260	8.33
10-0.30	990	990	2.97	297	7.92
10-0.35	943	943	2.83	330	7.55
10-0.40	901	901	2.70	360	7.21
15-0.25	1042	1042	3.12	260	8.33
15-0.30	990	990	2.97	297	7.92
15-0.35	943	943	2.83	330	7.55
15-0.40	901	901	2.70	360	7.21
20-0.25	1042	1041	3.12	260	8.33
20-0.30	990	990	2.97	297	7.92
20-0.35	943	943	2.83	330	7.55
20-0.40	901	901	2.70	360	7.21
25-0.25	1042	1042	3.12	260	8.33
25-0.30	990	990	2.97	297	7.92
25-0.35	943	943	2.83	330	7.55
25-0.40	901	901	2.70	360	7.21

An adhesion test developed by Li and Kwan (2011) was employed to measure the adhesiveness. In undergoing the test, several stone rods were immersed into the mortar mix to a depth of 100 mm and then gently lifted up. The stone rod adhesion (SRA, expressed in g/cm^2) was calculated as the mass of mortar adhered to the stone rods divided by the surface area of the immersed part of the stone rods. The higher is the SRA value, the higher is the adhesiveness, and vice versa.

In this research, the concept of particle packing (Kwan et al., 2012, 2015) was extended to the solid system comprising sand, cement, and basalt fibers. The wet packing method, wherein the solids were mixed with water and SP to become under wet condition, was applied for measurement of the packing density of the solid system. Detailed procedures of the wet packing method have been published elsewhere and interested readers may refer to the related literature (Wong and Kwan, 2014; Li et al., 2019b). In brief, the wet packing method measures the maximum solid concentration achieved at various water contents as the packing density of the solid system.

2.4 Calculation of WFT

The WFT of each mortar mix can be evaluated in the following manner. The first step is to measure the maximum solid concentration (ϕ_{max}), or packing density, of the solids in the mortar. Then, the minimum voids ratio (u_{min}) (defined as the ratio of voids volume to solid volume of the mortar) can be calculated as

$$u_{min} = \frac{1-\phi_{max}}{\phi_{max}}. \tag{1}$$

From the value of u_{min}, the excess water ratio (u_w') can be determined as

$$u_w' = u_w - u_{min}, \tag{2}$$

where u_w is the ratio of water volume to solid volume. The excess water ratio u_w' has the physical meaning of being the ratio of excess water volume to solid volume of mortar. In the above, the water volume is the free water volume.

Besides, the SSA of the solids in the mortar (A_s) is evaluated per the following equation:

$$A_s = A_{sand}R_{sand} + A_{cement}R_{cement} + A_{BF}R_{BF}, \tag{3}$$

where A_{sand}, A_{cement}, and A_{BF} are the individual SSAs of sand, cement, and basalt fibers, respectively, and R_{sand}, R_{cement}, and R_{BF} are the individual volumetric ratios of sand, cement, and basalt fibers to the total solids, respectively.

Finally, the WFT of the mortar mix is obtained as

$$\mathrm{WFT}=\frac{u'_{\mathrm{w}}}{A_{\mathrm{s}}}. \tag{4}$$

Note that the WFT so obtained is actually the average thickness of water films coating the solids.

3 Fresh properties

Table 4 summarizes all the fresh properties. In general, regardless of the fiber length, upon increasing the water/cement ratio, the flow rate, spread, and slump all increased, showing that the water/cement ratio played positive roles in the dynamic and static flowability of fiber-reinforced mortar.

Table 4 Fresh properties of mortar mixes

Mix number	Flow rate (mL/s)	Spread (mm)	Slump (mm)	SSI (%)	SRA (g/cm^2)
5-0.25	0	4	15	0.0	0.019
5-0.30	122	79	38	0.0	0.171
5-0.35	321	154	49	1.2	0.139
5-0.40	518	199	55	7.7	0.114
10-0.25	0	3	12	0.0	0.018
10-0.30	104	67	35	0.0	0.117
10-0.35	307	146	47	0.8	0.110
10-0.40	504	191	51	4.3	0.077
15-0.25	0	2	10	0.0	0.014
15-0.30	98	62	34	0.0	0.079
15-0.35	284	129	46	0.6	0.098
15-0.40	478	176	48	4.1	0.074
20-0.25	0	0	6	0.0	0.012
20-0.30	92	55	31	0.0	0.076
20-0.35	271	123	44	0.2	0.079
20-0.40	459	159	45	3.1	0.064
25-0.25	0	0	6	0.0	0.009
25-0.30	87	44	29	0.0	0.036
25-0.35	255	103	40	0.2	0.064
25-0.40	436	154	42	2.1	0.053

On the contrary, the SSI remained close to 0% when the water/cement ratio was relatively low, but began to increase when the water/cement ratio exceeded a certain value, indicating that there existed a threshold of water/cement ratio for the SSI to become sensitive to the cohesiveness and that the water/cement ratio played a negative role in the cohesiveness of fiber-reinforced mortar. However, the SRA varied with the water/cement ratio in a different manner. The SRA increased with the water/cement ratio when the water/cement ratio was relatively low, but after attaining a certain peak value at a water/cement ratio of 0.30 or 0.35, the SRA decreased as the water/cement ratio further increased. This indicates that the water/cement ratio played a complex positive or negative role in the adhesiveness, and there existed an optimal water/cement ratio for the maximum adhesiveness.

The fiber length also played key roles in the fresh properties. At a given water/cement ratio, upon increasing the fiber length, the flow rate, spread, and slump all decreased. This suggests that the fiber length played negative roles in the dynamic and static flowability of fiber-reinforced mortar. It is postulated that these adverse effects of the increased fiber length on the dynamic and static flowability were due to the hindrance of the fibers against flow and deformation of the mortar.

At the same time, the SSI decreased indicating a higher cohesiveness whereas the SRA decreased indicating a lower adhesiveness. Hence, upon increasing the fiber length, the cohesiveness increased but the adhesiveness decreased. It is postulated that the beneficial effect of the increased fiber length on the cohesiveness was due to pulling together of the mortar matrix by the fibers, and the adverse effect of the increased fiber length on the adhesiveness was due to worsening of the wall effect at the boundaries due to the presence of fibers, which decreased the packing density at the boundaries (Powers, 1968). More discussions on these effects are presented in the following sections.

4 Packing density and WFT

Because the aggregate/cement ratio and fiber content were fixed and the basalt fiber length varied among 5, 10, 15, 20, and 25 mm, there were five different combinations of solid mixtures (sand+cement+basalt fibers). The packing densities of these five solid mixtures were measured, and the results are listed in Table 5 and plotted in Fig. 3.

Table 5 Packing density and WFT results of mortar mixes

Mix number	Packing density	Water ratio	Excess water ratio	SSA (m^2/m^3)	WFT (μm)
5-0.25	0.7443	0.3521	0.0086	900 062	0.0096
5-0.30		0.4225	0.0790		0.0878
5-0.35		0.4929	0.1494		0.1660
5-0.40		0.5633	0.2198		0.2442
10-0.25	0.7405	0.3521	0.0017	900 062	0.0019
10-0.30		0.4225	0.0721		0.0801
10-0.35		0.4929	0.1425		0.1583
10-0.40		0.5633	0.2129		0.2365
15-0.25	0.7392	0.3521	−0.0007	900 062	−0.0008
15-0.30		0.4225	0.0697		0.0774
15-0.35		0.4929	0.1401		0.1557
15-0.40		0.5633	0.2105		0.2339
20-0.25	0.7367	0.3521	−0.0053	900 062	−0.0059
20-0.30		0.4225	0.0651		0.0723
20-0.35		0.4929	0.1355		0.1505
20-0.40		0.5633	0.2059		0.2288
25-0.25	0.7343	0.3521	−0.0097	900 062	−0.0108
25-0.30		0.4225	0.0607		0.0674
25-0.35		0.4929	0.1311		0.1457
25-0.40		0.5633	0.2015		0.2239

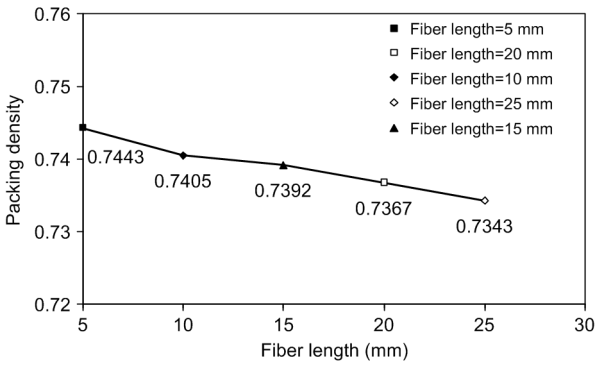

Fig. 3 Packing density versus basalt fiber length

It is noted that upon increasing the fiber length from 5 to 25 mm, the packing density decreased from 0.7443 to 0.7343. The corresponding voids ratio, as computed using Eq. (1), increased from 0.3435 to 0.3618. Such phenomenon may be explicated as follows: though the fibers had a small diameter and were flexible enough to readily pass through or penetrate into the voids between the sand grains, certain parts of isolated fibers could be entrapped within the narrow gaps between the sand grains especially when the fibers were relatively long. As a consequence, the sand grains were wedged apart so that the inter-particle distance was increased (this is called the wedging effect), thus causing the voids ratio to increase and the packing density to decrease (Kwan et al., 2013; Li et al., 2019b, 2019c).

The results of the water ratio and excess water ratio are reported in the third and fourth columns of Table 5, respectively. These are in line with the expectation that due to the higher water content, the water ratio and excess water ratio increased with the water/cement ratio. In the table, some of the excess water ratios are presented as negative values (the excess water ratios of mortar mixes 15-0.25, 20-0.25, and 25-0.25). These negative values mean that in these mortar mixes, the water added was not sufficient to fill up the voids, thereby leading to the presence of air in the voids within the solid skeleton. Similar phenomena had also been found in other studies (Li and Kwan, 2011; Wu and An, 2014).

In addition, the SSAs of the five solid mixtures are shown in the penultimate column of Table 5. Because the fiber content and aggregate/cement ratio were constant in this study, the SSAs of these solid mixtures were all equal to 900 062 m^2/m^3. Lastly, the WFTs, calculated as per Eq. (4), are presented in the last column of Table 5 and plotted versus the fiber length in Fig. 4. The WFT results reveal that among the mortar mixes tested, the WFT ranged from −0.0108 to 0.2442 μm. Some WFT values were negative because the corresponding excess water ratios were negative. Regardless of the water/cement ratio (W/C), the WFT decreased as the fiber length increased, which was caused by the decrease in packing density and the increase in voids ratio.

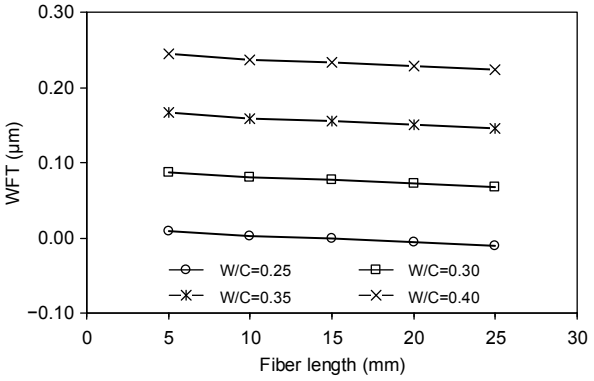

Fig. 4 WFT versus basalt fiber length with different water/cement ratios (W/C in short)

5 Roles of fiber length and WFT

5.1 Roles in dynamic flowability

To investigate how the fiber length and WFT affected the dynamic flowability, the flow rate versus the WFT is plotted in Fig. 5. It is clear that when the WFT was around 0 μm, the flow rate remained at 0 mL/s, but once the WFT became larger than a certain positive value, the flow rate increased in an approximately linear manner with the WFT. Overall, increasing the WFT led to significant improvement of the flow rate, meaning that the WFT played a major role in the dynamic flowability. Besides, the results indicate that at a given WFT, a longer fiber length generally led to a lower flow rate. It means that apart from the WFT, the fiber length also had a direct but adverse effect on the dynamic flowability. The possible causes were the intertwining of the fibers and the hindrance of the fibers against the dynamic flow of the mortar mix, especially when the fiber length was relatively long.

For analyzing the integrated roles of the fiber length and WFT, the best-fit curves for the flow rate–WFT relation at different fiber lengths are derived by performing numerical regression, as plotted in Fig. 5 juxtaposing with the data points. A very high R^2 value (i.e. coefficient of determination) of 0.992 is achieved, showing that the flow rate is controlled by both the fiber length and WFT. It is also evident that when longer basalt fibers are used, the curve shifts downwards such that at a given WFT, the dynamic flowability becomes lower. Hence, in applications where a high flow rate is needed, such as fiber-reinforced mortar/concrete to be pumped, the fiber length should not be too long.

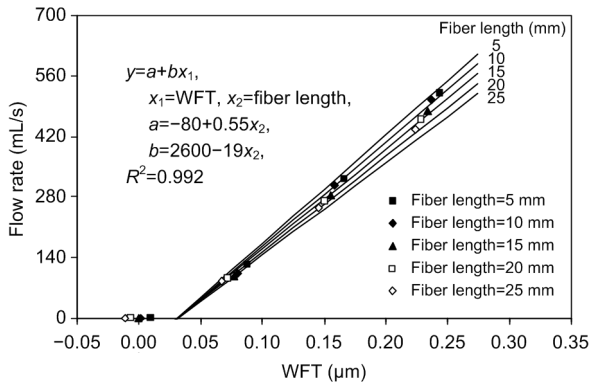

Fig. 5 Flow rate versus WFT

5.2 Roles in static flowability

To study how the fiber length and WFT influenced the static flowability, the spread and slump versus the WFT are plotted in Figs. 6 and 7, respectively. It is noted that in general, increasing the WFT led to increases of the spread and slump at gradually diminishing rates. At a WFT of beyond 0.25 μm, any further increase in the WFT produced only marginal increases in the spread and slump. On the whole, the static flowability significantly increased with the WFT, revealing that the WFT had major influence on the static flowability. Besides, regardless of the WFT, a longer fiber length always impaired the spread and slump. Therefore, the fiber length also had a direct but adverse effect on the static flowability. As in the case of dynamic flowability, the possible causes were the intertwining of the fibers and the hindrance of the fibers against the static flow and deformation of the mortar mix, especially when the fiber length was relatively long.

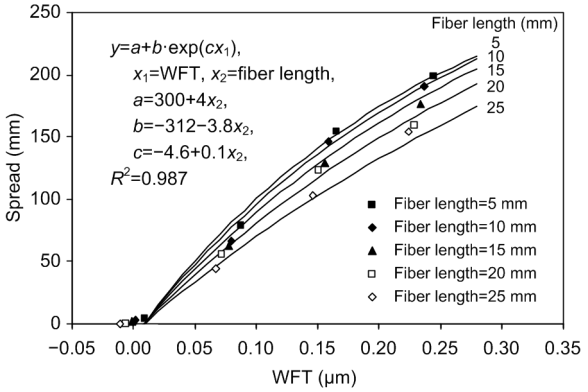

Fig. 6 Spread versus WFT

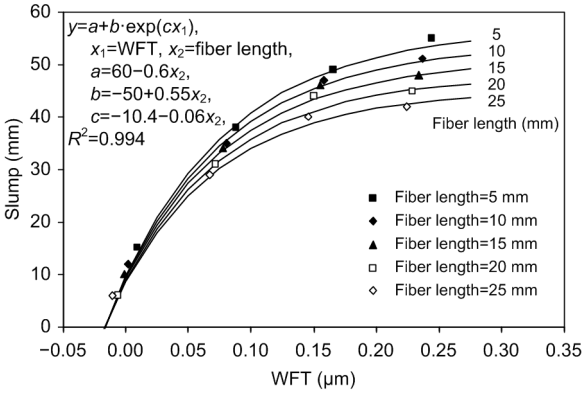

Fig. 7 Slump versus WFT

For quantifying the integrated effects of the fiber length and WFT, numerical regression is conducted, and the best-fit curves for the spread–WFT and slump–WFT relations at different fiber lengths are derived, as plotted alongside the data points in Figs. 6 and 7, respectively. Very high R^2 values of 0.987 and 0.994 are achieved, demonstrating that the fiber length and WFT are together the governing factors controlling the spread and slump. It is also clear that when longer basalt fibers are used, the curve shifts downwards such that at a given WFT, the static flowability becomes lower. Hence, in applications where high spread and slump are needed, such as self-levelling or self-compacting fiber-reinforced mortar/concrete, the fiber length should not be too long.

5.3 Roles in cohesiveness

To better reveal how the fiber length and WFT affected the cohesiveness, the SSI versus the WFT is plotted in Fig. 8. From the figure, it is apparent that within the range of WFT from slightly negative to 0.10 μm, the SSI was very low, but once the WFT exceeded a certain value of about 0.15 μm, the SSI increased sharply with the WFT. Since the SSI is inversely related to the cohesiveness, this implies that the cohesiveness decreased as the WFT increased and that the WFT played a major but detrimental role in the cohesiveness. In addition, it is noted that at a given WFT, increasing the fiber length greatly reduced the SSI, meaning that the fiber length played a beneficial role in the cohesiveness. The possible causes were the intertwining of the fibers and the pulling together of the mortar matrix by the fibers, especially when the fiber length was relatively long.

For evaluating the integrated influences of the fiber length and WFT, the best-fit curves for the SSI–WFT relation at different fiber lengths are derived by numerical regression, as plotted in Fig. 8. A very high R^2 value of 0.987 is obtained, meaning that the SSI or cohesiveness is governed jointly by the fiber length and WFT. It is also seen that as the fiber length increases, the curve shifts downwards, revealing that at the same WFT, the SSI decreases and the cohesiveness increases when longer basalt fibers are used. Hence, whilst a longer fiber length would decrease the dynamic and static flowability, it has the advantage of increasing the cohesiveness, which may be important in certain applications, such as self-compacting fiber-reinforced mortar/concrete, where a high cohesiveness is needed to pull the aggregate particles through narrow gaps to impart a high passing ability.

5.4 Roles in adhesiveness

To show how the fiber length and WFT influenced the adhesiveness, the SRA versus the WFT is plotted in Fig. 9. It is seen that when the WFT was close to 0.0 μm, the SRA was rather low; when the WFT was increased to around 0.05 to 0.15 μm, the SRA attained the peak value depending on the fiber length; but subsequent to attaining the peak, the SRA decreased as the WFT further increased. The reasons are explicated as follows: at a very small WFT, the mortar was not wet enough to adhere to the stone surfaces, while as the WFT increased, the mortar became sufficiently wet to adhere to the stone surfaces. However, when the WFT were increased further, the mortar became too wet and had a tendency to drip downwards from the stone surfaces.

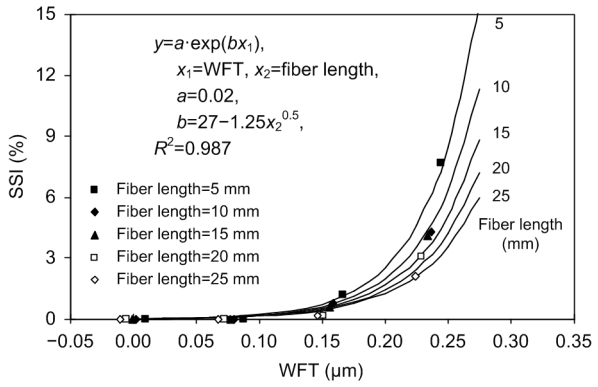

Fig. 8 SSI versus WFT

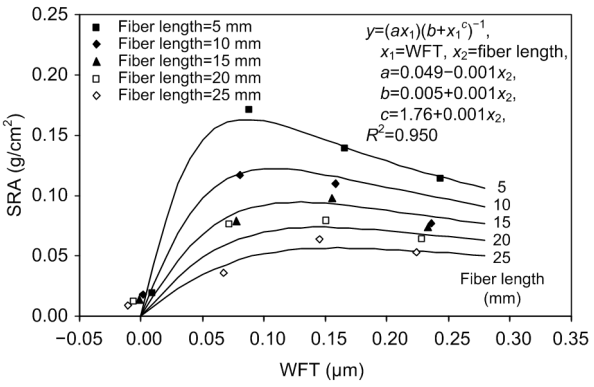

Fig. 9 SRA versus WFT

The SRA was dependent also on the fiber length. In general, at a given WFT, a longer fiber length tended to significantly lower the SRA. This was because firstly, the fibers could not penetrate through the stone surfaces to help adhere the mortar onto the stone surfaces, and secondly, when the mortar dripped downwards, the fibers actually dragged the mortar downwards leaving less mortar adhering on the stone surfaces. Moreover, from the particle packing point of view, the wall effect should have occurred at the stone surfaces causing the packing density to be reduced there (Powers, 1968). The presence of fibers might have further loosened the packing at the stone surfaces to decrease the number of contact points between the particles and the stone surfaces and thus reduced the adhesion. Hence, the addition of basalt fibers, especially long basalt fibers, would not improve the adhesiveness and in fact would reduce the adhesiveness of the mortar, despite the positive effect on the cohesiveness.

For analyzing the integrated effects of the fiber length and WFT, the best-fit curves for the SRA–WFT relation at different fiber lengths are determined by numerical regression, as plotted in Fig. 9. A high R^2 value of 0.950 is attained, reflecting that the SRA is governed jointly by the fiber length and WFT. It is also important to note that increasing the fiber length would shift the curve downwards, resulting in a lower SRA at a given WFT. Hence, in applications where a high adhesiveness is needed, such as fiber-reinforced mortar for rendering and spraying, the fiber length should not be too long and the WFT should be optimized to maximize the adhesiveness for replenishing the loss in adhesiveness due to the addition of fibers.

6 Effects of fiber length at different WFTs

6.1 Effects on dynamic and static flowability

For the purpose of isolating the effects of the fiber length on the dynamic and static flowability, the percentage reductions in the flow rate, spread, and slump are calculated using the best-fit equations obtained previously and plotted against the fiber length for different WFT values in Figs. 10, 11, and 12, respectively. Evidently, the percentage reductions in flow rate, spread, and slump are dependent on the WFT but are generally larger at longer fiber length. Particularly, the percentage reduction in flow rate increases with the fiber length at a constant rate, the percentage reduction in spread increases with the fiber length at a gradually increasing rate, and the percentage reduction in slump increases with the fiber length at an approximately constant rate. For instance, at a constant WFT of 0.05 μm, a fiber length of 25 mm reduces the flow rate by up to 20.1%, the spread by up

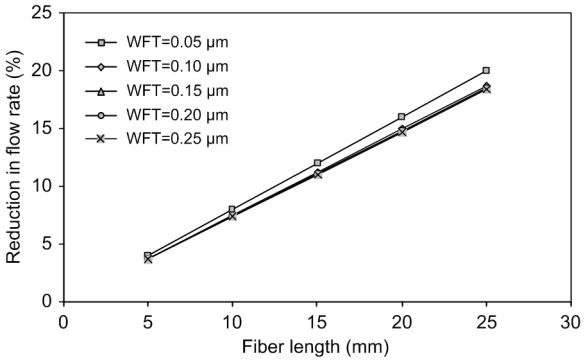

Fig. 10 Percentage reduction in flow rate versus basalt fiber length

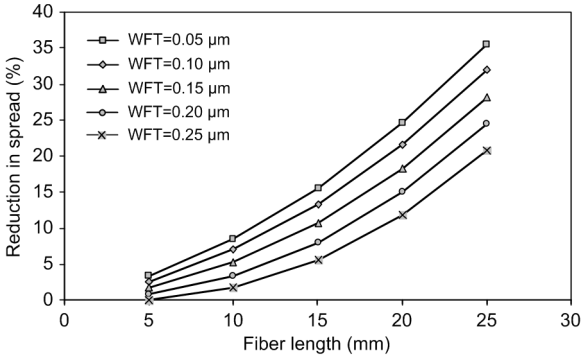

Fig. 11 Percentage reduction in spread versus basalt fiber length

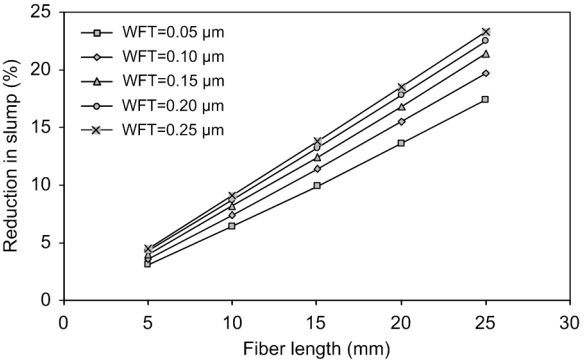

Fig. 12 Percentage reduction in slump versus basalt fiber length

to 35.6%, and the slump by up to 17.4%. Relatively, a shorter fiber length of 20 mm reduces the flow rate, spread, and slump by smaller percentages.

6.2 Effects on cohesiveness and adhesiveness

Likewise, for the purpose of isolating the effects of the fiber length on the cohesiveness and adhesiveness, the percentage changes in the SSI and SRA are calculated using the best-fit equations obtained previously and plotted against the fiber length for different WFT values in Figs. 13 and 14, respectively. As for the dynamic and static flowability, the percentage reductions in SSI and SRA are dependent on the WFT but are generally larger at longer fiber lengths. Particularly, the percentage reductions in SSI and SRA increase with the fiber length at gradually decreasing rates. Overall, at a constant WFT, a relatively long fiber length of 25 mm causes substantial reductions in both the SSI and SRA, or in other words, substantial increase in the cohesiveness but also substantial decrease in the adhesiveness.

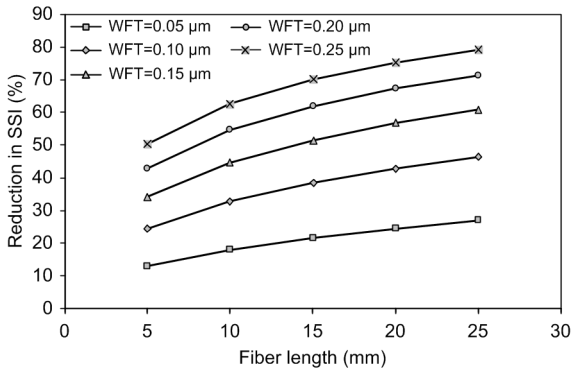

Fig. 13 Percentage reduction in SSI versus basalt fiber length

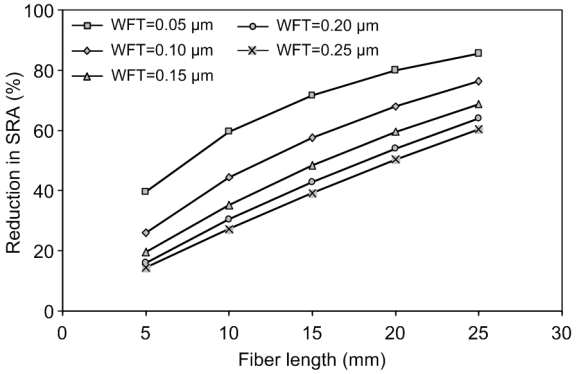

Fig. 14 Percentage reduction in SRA versus basalt fiber length

6.3 Comparison with previous findings in the literature

The effects of fiber length on the dynamic and static flowability described above are generally in line with the previous findings in the literature that the use of longer fibers would increase the viscosity (Banfill et al., 2006; Poznyak et al., 2014) and decrease the passing ability (Ghernouti et al., 2015). However, the effects of fiber length on cohesiveness and adhesiveness cannot be compared with previous findings because there have been little similar studies. Finally, it is emphasized that the best-fit curves obtained herein would improve our understanding of the rheology of basalt fiber-reinforced mortar and assist the selection of fiber length in the design of various types of basalt fiber-reinforced mortar. As a direction for future development, extension of this research program to encompass different types of fibers is recommended.

7 Conclusions

A systematic experimental research program aiming to study the influences of fiber length and WFT on the fresh properties of basalt fiber-reinforced mortar has been completed. In this study, the fiber length was varied from 5 to 25 mm and the water/cement ratio was varied from 0.25 to 0.40. Based on the test results, the following conclusions are drawn:

1. Apart from plain mortar, the concept of WFT is confirmed to be applicable also to basalt fiber-reinforced mortar. Generally, the fiber length plays negative roles in the packing density and WFT, whilst both the fiber length and WFT have major influences on the fresh properties of the fiber-reinforced mortar.

2. A larger WFT has beneficial effects on the dynamic and static flowability but adverse effect on the cohesiveness. However, it could have beneficial or adverse effect on the adhesiveness because there is an optimal WFT for maximum adhesiveness. On the other hand, the fiber length has adverse effects on the dynamic and static flowability, beneficial effect on the cohesiveness, and quite unexpectedly, adverse effect on the adhesiveness.

3. The flow rate, spread, slump, SSI, and SRA have been correlated by regression analysis to the

fiber length and WFT, and very high R^2 values (i.e. values of coefficient of determination) of at least 0.950 have been obtained, indicating that the fiber length and WFT are together the major factors governing these fresh properties.

4. From the afore-mentioned regression analysis, best-fit curves and equations correlating the flow rate, spread, slump, SSI, and SRA to the fiber length and WFT have been derived, from which the roles of the fiber length and WFT can be clearly seen. Overall, the fiber length exerts its influence through both the indirect effects on the packing density and WFT and the direct effect on fiber-mortar interaction.

5. The percentage changes in the flow rate, spread, slump, SSI, and SRA due to the presence of basalt fibers with different fiber lengths have been calculated and plotted to reveal the actual effects of the fiber length at various WFTs. The curves plotted are useful reference for selecting a suitable fiber length in the mix design of various types of basalt fiber-reinforced mortar.

In theory, the graphs in Figs. 5–9, which give the fresh properties in terms of the fiber length and WFT, may also be used as design charts for the mix design of basalt fiber-reinforced mortar. However, these are strictly applicable to mortar mixes using similar materials and having more or less the same aggregate/cement ratio and fiber content. Hence, at this stage, these graphs may only be used as general guidelines for preliminary mix design or development of design charts based on the test results obtained from trial mortar mixing. Further research taking into account also the effects of fiber type, fiber content, aggregate size, and aggregate content is needed to develop a comprehensive rheological model for fiber-reinforced mortar.

Contributors

Leo Gu LI wrote the first draft of the manuscript. Yi OUYANG processed the corresponding data. Pui-Lam NG revised and edited the final version. Kai-long ZENG carried out the investigation. Albert Kwok Hung KWAN gave the conceptualization.

Conflict of interest

Leo Gu LI, Yi OUYANG, Pui-Lam NG, Kai-long ZENG, and Albert Kwok Hung KWAN declare that they have no conflict of interest.

References

Abbass W, Khan MI, Mourad S, 2018. Evaluation of mechanical properties of steel fiber reinforced concrete with different strengths of concrete. *Construction and Building Materials*, 168:556-569. https://doi.org/10.1016/j.conbuildmat.2018.02.164

Ahari RS, 2018. Role of water film thickness on rheological characteristics of self-consolidating concrete containing silica fume. *Journal of New Approaches in Civil Engineering*, 2(2):1-10. https://doi.org/10.30469/jnace.2018.69390

Ali M, Liu A, Sou H, et al., 2012. Mechanical and dynamic properties of coconut fibre reinforced concrete. *Construction and Building Materials*, 30:814-825. https://doi.org/10.1016/j.conbuildmat.2011.12.068

AQSIQ (General Administration of Quality Supervision, Inspection and Quarantine of the People's Republic of China), 2007. Common Portland Cement, GB 175–2007. Standardization Administration of China, Beijing, China (in Chinese).

Banfill PFG, 1994. Rheological methods for assessing the flow properties of mortar and related materials. *Construction and Building Materials*, 8(1):43-50. https://doi.org/10.1016/0950-0618(94)90007-8

Banfill PFG, Starrs G, Derruau G, et al., 2006. Rheology of low carbon fibre content reinforced cement mortar. *Cement and Concrete Composites*, 28(9):773-780. https://doi.org/10.1016/j.cemconcomp.2006.06.004

CEN (European Committee for Standardization), 2010a. Testing Fresh Concrete–Part 9: Self-compacting Concrete–V-funnel Test, EN 12350-9:2010. CEN, Brussels, Belgium.

CEN (European Committee for Standardization), 2010b. Testing Fresh Concrete–Part 11: Self-compacting Concrete–Sieve-segregation Test, EN 12350-11:2010. CEN, Brussels, Belgium.

CEN (European Committee for Standardization), 2019. Testing Fresh Concrete–Part 8: Self-compacting Concrete–Slump-flow Test, EN 12350-8:2019. CEN, Brussels, Belgium.

Chen JJ, Ng PL, Kwan AKH, et al., 2019. Lowering cement content in mortar by adding superfine zeolite as cement replacement and optimizing mixture proportions. *Journal of Cleaner Production*, 210:66-76. https://doi.org/10.1016/j.jclepro.2018.11.007

Chen JJ, Ng PL, Chu SH, et al., 2020. Ternary blending with metakaolin and silica fume to improve packing density and performance of binder paste. *Construction and Building Materials*, 252:119031. https://doi.org/10.1016/j.conbuildmat.2020.119031

Chu SH, Li LG, Kwan AKH, 2018. Fibre factors governing the fresh and hardened properties of steel FRC. *Construction and Building Materials*, 186:1228-1238. https://doi.org/10.1016/j.conbuildmat.2018.08.047

Claisse PA, Lorimer P, Al Omari M, 2001. Workability of cement pastes. *ACI Materials Journal*, 98(6):476-482.

https://doi.org/10.14359/10849

Cordeiro GC, Toledo Filho RD, Tavares LM, et al., 2011. Influence of particle size and specific surface area on the pozzolanic activity of residual rice husk ash. *Cement and Concrete Composites*, 33(5):529-534. https://doi.org/10.1016/j.cemconcomp.2011.02.005

de Schutter G, Bartos PJM, Domone P, et al., 2008. Self-compacting Concrete. CRC Press, Boca Raton, USA, p.296.

Eidan J, Rasoolan I, Rezaeian A, et al., 2019. Residual mechanical properties of polypropylene fiber-reinforced concrete after heating. *Construction and Building Materials*, 198:195-206. https://doi.org/10.1016/j.conbuildmat.2018.11.209

Felekoğlu B, Türkel S, Baradan B, 2007. Effect of water/cement ratio on the fresh and hardened properties of self-compacting concrete. *Building and Environment*, 42(4):1795-1802. https://doi.org/10.1016/j.buildenv.2006.01.012

Ghernouti Y, Rabehi B, Bouziani T, et al., 2015. Fresh and hardened properties of self-compacting concrete containing plastic bag waste fibers (WFSCC). *Construction and Building Materials*, 82:89-100. https://doi.org/10.1016/j.conbuildmat.2015.02.059

Gribniak V, Arnautov AK, Kaklauskas G, et al., 2015. Investigation on application of basalt materials as reinforcement for flexural elements of concrete bridges. *The Baltic Journal of Road and Bridge Engineering*, 10(3):201-206. https://doi.org/10.3846/bjrbe.2015.25

Hunger M, Brouwers HJH, 2009. Flow analysis of water–powder mixtures: application to specific surface area and shape factor. *Cement and Concrete Composites*, 31(1):39-59. https://doi.org/10.1016/j.cemconcomp.2008.09.010

Islam MS, Ahmed SJU, 2018. Influence of jute fiber on concrete properties. *Construction and Building Materials*, 189:768-776. https://doi.org/10.1016/j.conbuildmat.2018.09.048

Kismi M, Saint-Arroman JC, Mounanga P, 2012. Minimizing water dosage of superplasticized mortars and concretes for a given consistency. *Construction and Building Materials*, 28(1):747-758. https://doi.org/10.1016/j.conbuildmat.2011.10.056

Kwan AKH, Li LG, 2012. Combined effects of water film thickness and paste film thickness on rheology of mortar. *Materials and Structures*, 45(9):1359-1374. https://doi.org/10.1617/s11527-012-9837-y

Kwan AKH, Li LG, 2014. Combined effects of water film, paste film and mortar film thicknesses on fresh properties of concrete. *Construction and Building Materials*, 50:598-608. https://doi.org/10.1016/j.conbuildmat.2013.10.014

Kwan AKH, Fung WWS, Wong HHC, 2010. Water film thickness, flowability and rheology of cement-sand mortar. *Advances in Cement Research*, 22(1):3-14. https://doi.org/10.1680/adcr.2008.22.1.3

Kwan AKH, Li LG, Fung WWS, 2012. Wet packing of blended fine and coarse aggregate. *Materials and Structures*, 45(6):817-828. https://doi.org/10.1617/s11527-011-9800-3

Kwan AKH, Chan KW, Wong V, 2013. A 3-parameter particle packing model incorporating the wedging effect. *Powder Technology*, 237:172-179. https://doi.org/10.1016/j.powtec.2013.01.043

Kwan AKH, Wong V, Fung WWS, 2015. A 3-parameter packing density model for angular rock aggregate particles. *Powder Technology*, 274:154-162. https://doi.org/10.1016/j.powtec.2014.12.054

Li LG, Kwan AKH, 2011. Mortar design based on water film thickness. *Construction and Building Materials*, 25(5):2381-2390. https://doi.org/10.1016/j.conbuildmat.2010.11.038

Li LG, Kwan AKH, 2013. Concrete mix design based on water film thickness and paste film thickness. *Cement and Concrete Composites*, 39:33-42. https://doi.org/10.1016/j.cemconcomp.2013.03.021

Li LG, Kwan AKH, 2014. Packing density of concrete mix under dry and wet conditions. *Powder Technology*, 253:514-521. https://doi.org/10.1016/j.powtec.2013.12.020

Li LG, Kwan AKH, 2017. Roles of superplasticiser dosage, water film thickness and slurry film thickness in flowability of cementitious paste. *Advances in Cement Research*, 29(7):287-301. https://doi.org/10.1680/jadcr.16.00187

Li LG, Lin CJ, Chen GM, et al., 2017a. Effects of packing on compressive behaviour of recycled aggregate concrete. *Construction and Building Materials*, 157:757-777. https://doi.org/10.1016/j.conbuildmat.2017.09.097

Li LG, Zhu J, Zhao ZW, et al., 2017b. Roles of water film thickness and polypropylene fibre content in fresh properties of mortar. *Advances in Cement Research*, 29(2):71-80. https://doi.org/10.1680/jadcr.16.00102

Li LG, Zhao ZW, Zhu J, et al., 2018a. Combined effects of water film thickness and polypropylene fibre length on fresh properties of mortar. *Construction and Building Materials*, 174:586-593. https://doi.org/10.1016/j.conbuildmat.2018.03.259

Li LG, Chu SH, Zeng KL, et al., 2018b. Roles of water film thickness and fibre factor in workability of polypropylene fibre reinforced mortar. *Cement and Concrete Composites*, 93:196-204. https://doi.org/10.1016/j.cemconcomp.2018.07.014

Li LG, Zeng KL, Ouyang Y, et al., 2019a. Basalt fibre-reinforced mortar: rheology modelling based on water film thickness and fibre content. *Construction and Building Materials*, 229:116857. https://doi.org/10.1016/j.conbuildmat.2019.116857

Li LG, Zhuo HX, Zhu J, et al., 2019b. Packing density of mortar containing polypropylene, carbon or basalt fibres under dry and wet conditions. *Powder Technology*, 342:

433-440.
https://doi.org/10.1016/j.powtec.2018.10.005

Li LG, Huang ZH, Tan YP, et al., 2019c. Recycling of marble dust as paste replacement for improving strength, microstructure and eco-friendliness of mortar. *Journal of Cleaner Production*, 210:55-65.
https://doi.org/10.1016/j.jclepro.2018.10.332

Li LG, Ouyang Y, Zhuo ZY, et al., 2021a. Adding ceramic polishing waste as filler to reduce paste volume and improve carbonation and water resistances of mortar. *Advances in Bridge Engineering*, 2:3.
https://doi.org/10.1186/s43251-020-00019-2

Li LG, Xiao BF, Fang ZQ, et al., 2021b. Feasibility of glass/basalt fiber reinforced seawater coral sand mortar for 3D printing. *Additive Manufacturing*, 37:101684.
https://doi.org/10.1016/j.addma.2020.101684

Li LG, Feng JJ, Zhu J, et al., 2021c. Pervious concrete: effects of porosity on permeability and strength. *Magazine of Concrete Research*, 73(2):69-79.
https://doi.org/10.1680/jmacr.19.00194

Li LG, Zheng JY, Ng PL, et al., 2021d. Synergistic cementing efficiencies of nano-silica and micro-silica in carbonation resistance and sorptivity of concrete. *Journal of Building Engineering*, 33:101862.
https://doi.org/10.1016/j.jobe.2020.101862

Mehdipour I, Khayat KH, 2017. Effect of particle-size distribution and specific surface area of different binder systems on packing density and flow characteristics of cement paste. *Cement and Concrete Composites*, 78:120-131.
https://doi.org/10.1016/j.cemconcomp.2017.01.005

Midorikawa T, Pelova GI, Walraven JC, 2009. Application of "the water layer model" to self-compacting mortar with different size distributions of fine aggregate. *Heron*, 54(2-3):73-99.

Ng PL, Kwan AKH, Li LG, 2016. Packing and film thickness theories for the mix design of high-performance concrete. *Journal of Zhejiang University-SCIENCE A (Applied Physics & Engineering)*, 17(10):759-781.
https://doi.org/10.1631/jzus.A1600439

Okamura H, Ouchi M, 2003. Self-compacting concrete. *Journal of Advanced Concrete Technology*, 1(1):5-15.
https://doi.org/10.3151/jact.1.5

Powers TC, 1968. The Properties of Fresh Concrete. John Wiley & Sons, New York, USA, p.664.

Poznyak OR, Kirakevych II, Stechyshyn MS, 2014. Properties of self-compacting concrete with basalt fiber. *Academic Journals & Conferences of Lviv Polytechnic National University*, (781):149-154.

Shi CJ, Jiao DW, Zhang J, et al., 2018. Design of high performance concrete with multiple performance requirements for #2 Dongting Lake Bridge. *Construction and Building Materials*, 165:825-832.
https://doi.org/10.1016/j.conbuildmat.2018.01.083

Sun Y, Wang ZL, Gao QF, et al., 2018. A new mixture design methodology based on the packing density theory for high performance concrete in bridge engineering. *Construction and Building Materials*, 182:80-93.
https://doi.org/10.1016/j.conbuildmat.2018.06.062

Wong HHC, Kwan AKH, 2008. Rheology of cement paste: role of excess water to solid surface area ratio. *Journal of Materials in Civil Engineering*, 20(2):189-197.
https://doi.org/10.1061/(asce)0899-1561(2008)20:2(189)

Wong V, Kwan AKH, 2014. A 3-parameter model for packing density prediction of ternary mixes of spherical particles. *Powder Technology*, 268:357-367.
https://doi.org/10.1016/j.powtec.2014.08.036

Wu Q, An XH, 2014. Development of a mix design method for SCC based on the rheological characteristics of paste. *Construction and Building Materials*, 53:642-651.
https://doi.org/10.1016/j.conbuildmat.2013.12.008

Wu Q, An XH, Liu CN, 2014. Effect of polycarboxylate-type superplasticizer on the paste fluidity based on the water film thickness of flocs. *Science China Technological Sciences*, 57(8):1522-1531.
https://doi.org/10.1007/s11431-014-5594-1

Yu AB, Bridgwater J, Burbidge A, 1997. On the modelling of the packing of fine particles. *Powder Technology*, 92(3):185-194.
https://doi.org/10.1016/S0032-5910(97)03219-1

Zhang RX, Panesar DK, 2017. New approach to calculate water film thickness and the correlation to the rheology of mortar and concrete containing reactive MgO. *Construction and Building Materials*, 150:892-902.
https://doi.org/10.1016/j.conbuildmat.2017.05.218